Novel Water-Mediated Hydrogen Bonds as the Structural Basis for the Low Oxygen Affinity of the Blood Substitute Candidate rHb(α96Val→Trp)[†,‡]

Yoram A. Puius,[§] Ming Zou,[||] Nancy T. Ho,[||] Chien Ho,[||] and Steven C. Almo*[,§]

Department of Biochemistry, Albert Einstein College of Medicine, Bronx, New York 10461, and Department of Biological Sciences, Carnegie Mellon University, 4400 Fifth Avenue, Pittsburgh, Pennsylvania 15213

Received November 3, 1997; Revised Manuscript Received February 5, 1998

ABSTRACT: One of the most promising approaches for the development of a synthetic blood substitute has been the engineering of novel mutants of human hemoglobin (Hb) A which maintain cooperativity, but possess lowered oxygen affinity. We describe here two crystal structures of one such potential blood substitute, recombinant (r) Hb(α96Val→Trp), refined to 1.9 Å resolution in an α-aquomet, β-deoxy T-state, and to 2.5 Å resolution in a carbonmonoxy R-state. On the basis of molecular dynamics simulations, a particular conformation had been predicted for the engineered Trp residue, and the lowered oxygen affinity had been attributed to a stabilization of the deoxy T-state interface by α96Trp−β99Asp hydrogen bonds. Difference Fourier maps of the T-state structure clearly show that α96Trp is in a conformation different from that predicted by the simulation, with its indole side chain directed away from the interface and into the central cavity. In this conformation, the indole nitrogen makes novel water-mediated hydrogen bonds across the T-state interface with β101Glu. We propose that these water-mediated hydrogen bonds are the structural basis for the lowered oxygen affinity of rHb(α96Val→Trp), and discuss the implications of these findings for future molecular dynamics studies and the design of Hb mutants.

The need for synthetic blood substitutes as a pathogen-free alternative to whole blood for use in emergency situations has long been recognized. One of the most promising approaches to the mimicry of hemoglobin (Hb) activity in the red cell is the use of solutions of hemoglobins which have been tailored, either through mutagenesis or chemical modification, to function as physiologically useful oxygen carriers (*1*−*3*). The realization of this goal may require the production of Hb molecules which bind oxygen cooperatively, have low oxygen affinity in the absence of allosteric effectors such as 2,3-diphosphoglycerate (2,3-DPG), and do not dissociate into dimers. Central to this effort is an atomic level understranding of the interactions of the subunit interfaces involved in switching between the liganded R-state and the unliganded T-state.

With the development of an expression system to produce normal adult human hemoglobin (Hb A) in *Escherichia coli* (*4*), several Hb mutants with high cooperativity and low O_2 affinity have been prepared and studied by biochemical and biophysical techniques (reviewed in ref *5*). One of these is rHb(α96Val→Trp), in which a valine located at the $\alpha_1-\beta_2$ subunit interface is replaced by a tryptophan (*6*). This recombinant hemoglobin exhibited a low oxygen affinity, almost identical to that of Hb A as measured in the presence of 5 mM 2,3-DPG, as well as high cooperativity in oxygen binding, with n_{max} values of 2.2−2.6 which compare favorably to a value of 3.0 for Hb A. ^{1}H NMR spectroscopy had suggested that the tertiary and quaternary structures of rHb(α96Val→Trp) are very similar to those of Hb A in both the deoxy and carbonmonoxy forms. An unusual feature of rHb(α96Val→Trp) was that the carbonmonoxy form could be converted to a ligated T-like quaternary structure by lowering the temperature or by adding the allosteric effector inositol hexaphosphate (IHP).

Preliminary molecular dynamics (MD) simulations had suggested that the unique oxygen-binding properties of rHb(α96Val→Trp) were due to the introduction of an additional hydrogen bond between the indole nitrogen of α96Trp and the carboxylate side chain of β99Asp across the $\alpha_1-\beta_2$ interface in the deoxy T-state. To experimentally verify the basis of the observed oxygen-binding properties, we undertook an X-ray crystallographic study of the T- and R-states.

We report here the crystal structure of rHb(α96Val→Trp) solved to 1.9 Å resolution in an α-met, β-deoxy T-state, and solved to 2.5 Å resolution in a carbonmonoxy R-state. We find that the tertiary and quaternary structures are, in general, similar to those of the corresponding Hb A structures. However, we also find that in the T-state structure, the engineered tryptophan residue is in a conformation different from that predicted by MD, with the indole side chain directed away from the interface and into the central cavity. The T-state structure does not possess the predicted hydrogen bond between α96Trp and β99Asp, but instead it demonstrates novel water-mediated hydrogen bonds between the indole nitrogen of α96Trp and β101Glu. These water-

[†] This work is supported by research grants from the National Institutes of Health (HL-24525 to C.H. and HL-58249 to C.H. and S.C.A.) Y.A.P. is supported by an M. S. T. P. grant from the N. I. H. (T32 GM07288).

[‡] The T-state and R-state structures have been deposited with the Brookhaven Protein Data Bank with accession numbers 1VWT and 1RVW, respectively.

* Corresponding author. E-mail: almo@aecom.yu.edu.

[§] Department of Biochemistry, Albert Einstein College of Medicine.

[||] Department of Biological Sciences, Carnegie Mellon University.

S0006-2960(97)02728-1 CCC: $15.00
Published on Web 06/12/1998

mediated hydrogen bonds appear to be the structural basis for the lowered oxygen affinity of rHb(α96Val→Trp). On the basis of this difference between simulation and experiment, we also present suggestions for the use of discrete water molecules in future molecular dynamics simulations.

EXPERIMENTAL PROCEDURES

Crystallization of rHb (α96Val→Trp) and Data Collection. Expression and purification of rHb (α96Val→Trp) was described previously by Kim et al. (*6*). Prior to crystallization, rHb (α96Val→Trp) was dialyzed against distilled deionized water and concentrated to 20 mg/mL. Crystals of the T-state and R-state structures were grown by the batch method of Perutz (*7*). For the T-state crystals, all steps of crystallization and mounting were performed inside a glovebag purged with nitrogen gas. The R-state crystals were flushed with CO during growth and mounting for data collection.

All data sets were collected at room temperature on a Siemens X-1000 multiwire area detector, using Cu Kα radiation from a Rigaku RU-200 X-ray generator operating in fine focus mode at 50 kV and 80 mA. The data were reduced with XDS and merged with XSCALE (*8*). Data were collected from a single crystal for each quaternary state.

Structure Solution and Refinement. The structures were solved by difference Fourier methods using T-state [1DXU (*9*)] or R-state [1HHO (*10*)] structures with the α96Val initially replaced by an alanine, and with the hemes omitted. Rigid-body, simulated annealing, positional, and temperature factor refinement with 8.0−1.9 Å (T-state) or 8.0−2.5 Å (R-state) data were performed with X-PLOR (*11*), accompanied by cycles of manual rebuilding with TOM (*12*) or O (*13*).

Hemes were initially built into OMIT map density without ligands, while in later cycles the water or carbon monoxide molecules were built into strong density in the T- and R-state structures, respectively (Figure 1). Ordered solvent molecules were placed in 3.0σ $F_o - F_c$ density with accompanying 1.0σ $2F_o - F_c$ density and were retained if their temperature factors refined to below 60 Å^2. At the final stages of refinement, tetrahedral density in $F_o - F_c$ simulated annealing maps were modeled as anions from the crystallization buffer: two sulfate ions in the T-state structure [as seen in 1DXU (*9*)] and a phosphate at a special position on a 2-fold axis in the R-state structure (Figure 6b) [as seen in 1HHO (*10*)].

In both structures, initial difference Fourier maps with α96 modeled as Ala immediately showed the Trp side chain density directed toward the central cavity. Simulated annealing OMIT maps (*14*) were calculated throughout the refinement procedure to confirm the position of α96Trp (Figure 2) and other residues, and the ligation state of the hemes (Figure 1). In the final refinement cycles, low-resolution data in the 25−8.0 Å range were included for the addition of an isotropic bulk solvent model (*15*). The stereochemical quality of the models was verified throughout refinement with the programs PROCHECK (*16*) and WHAT IF (*17*).

RESULTS

Quality of Crystal Structures. The T-state structure is very similar to the 1.74 Å wild-type deoxy Hb A structure 2HHB (*18*) as were previously described T-state α-met β-deoxy structures (*19*−*21*; reviewed in ref *22*). The R-state structure is similar to the 2.1 Å wild-type oxy Hb A structure 1HHO (*10*) (Table 1). (We typically used the oxy Hb A 1HHO for R-state comparisons instead of carbonmonoxy Hb A [2HCO (*23*)] because it was a higher-resolution structure with refined temperature factors.) Except where described below, the rHb

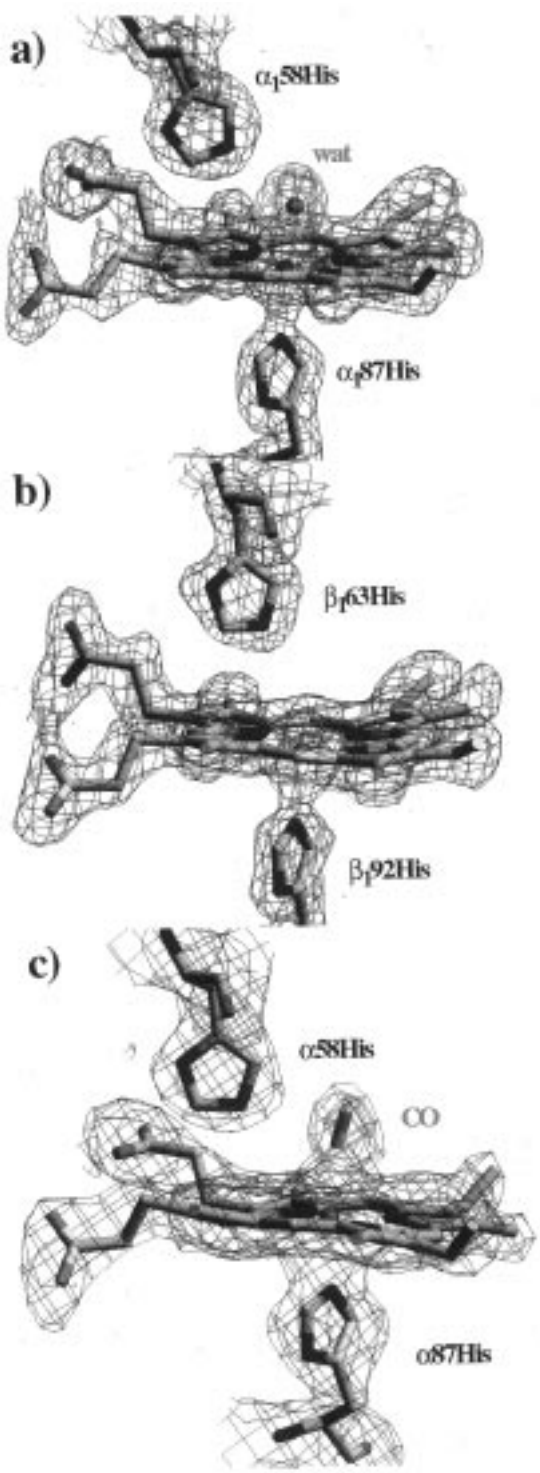

FIGURE 1: Heme ligands to the (a) α_1 heme of the T-state structure, (b) β_1 heme of the T-state structure, and (c) α heme of the R-state structure. Red contours are 4000K simulated annealing $F_o - F_c$ OMIT maps contoured at 3.0σ, blue contours are $2F_o - F_c$ OMIT maps contoured at 1.0σ. Figure produced with SETOR (*38*).

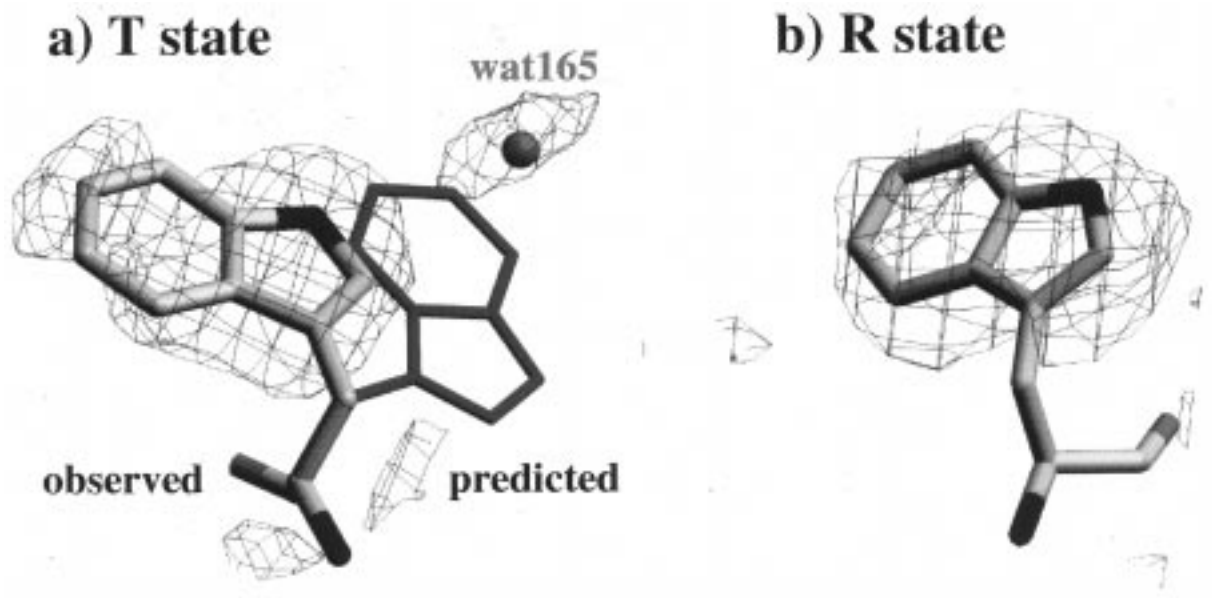

FIGURE 2: Conformation of α96Trp. (a) The conformation of $\alpha_1$96Trp in the T-state crystal structure, and the accompanying hydrogen-bonded water (red sphere). The predicted conformation is shown in green. (b) The conformation of α96Trp in the R-state structure. Blue contours show 4000K simulated annealing OMIT map $F_o - F_c$ density at 2.0σ. Figure produced with SETOR (*38*).

Table 1: Crystal Parameters, Data Collection and Refinement Statistics, and Structural Comparisons for rHb (α96Val→Trp)

	T-state (α-aquomet, β-deoxy)	R-state (carbonmonoxy)
crystal parameters		
space group	$P2_1$	$P4_12_12$
unit cell constants	$a = 63.27$ Å, $b = 83.41$ Å, $c = 53.79$ Å, $\beta = 99.54°$	$a = b = 54.28$ Å, $c = 194.12$ Å
contents of asymmetric unit	$\alpha_2\beta_2$ tetramer	$\alpha\beta$ dimer
data collection and refinement statistics		
resolution (Å)	25−1.9 (1.99−1.90)[a]	25−2.5 (2.61−2.50)
number of reflections	39 687 (4102)	9340 (993)
completeness (%)	91.3 (75.8)	86.7 (75.7)
R_{merge}[b] (%)	6.7	6.5
wavelength (Å)	1.54	1.54
crystallographic R[c] (%)	16.9 (22.7)	16.7 (24.1)
RMS deviation from ideality[d]		
bond length (Å)	0.009	0.008
bond angles (°)	1.2	1.3
number of non-hydrogen atoms		
protein	4398	2199
hemes	172	86
heme ligands	2 (2 H_2O)	4 (2 CO)
water molecules	241	25
anions	10 (2 SO_4)	5 (1 PO_4)
all atoms	4823	2319
avg temperature factors (Å^2)		
protein	20.4	33.7
hemes and ligands	18.0	31.3
water molecules	35.2	40.8
anions	18.7 (SO_4)	87.7 (PO_4)
all atoms	21.1	33.8
structural comparisons		
PDB entry for comparison	2HHB[e]	1HHO[f]
RMS difference[g] (Å) not including residue α96		
Cα atoms	0.16	0.41
all protein atoms	0.70	1.09

[a] Numbers in parentheses refer to the shell of highest-resolution data. [b] $R_{merge} = \sum_{hkl}\sum_n|\langle I(hkl)\rangle - I_n(hkl)|/\sum_{hkl}\sum_n I_n(hkl)$ where $I_n(hkl)$ and $\langle I(hkl)\rangle$ are the nth and mean measurements of the intensity of reflection hkl. [c] R factor $= \sum_{hkl}|F_o - F_c|/\sum_{hkl}F_o$ where F_o and F_c are the observed and calculated structure factor amplitudes for reflection hkl. [d] Stereochemical criteria are those of Engh and Huber (*36*). [e] Ref *18*. [f] Ref *10*. [g] Calculated with ProFitV1.6 (*37*).

(α96Val→Trp) structures are essentially identical to the wild-type equivalents.

As shown in Table 1, both structures refined with good *R*-factors (T-state, 16.9%; R-state, 16.7%) and good geometry (T-state, rmsd bond lengths 0.009 Å, rmsd bond angles 1.2°; R-state, rmsd bond lengths 0.008 Å, rmsd bond angles 1.3°) with the addition of appropriate solvent molecules (T-state, 241 H_2O, 2 SO_4; R-state, 25 H_2O, 1 PO_4). The ordered anions from the crystallization solutions had been previously observed (*9*, *10*).

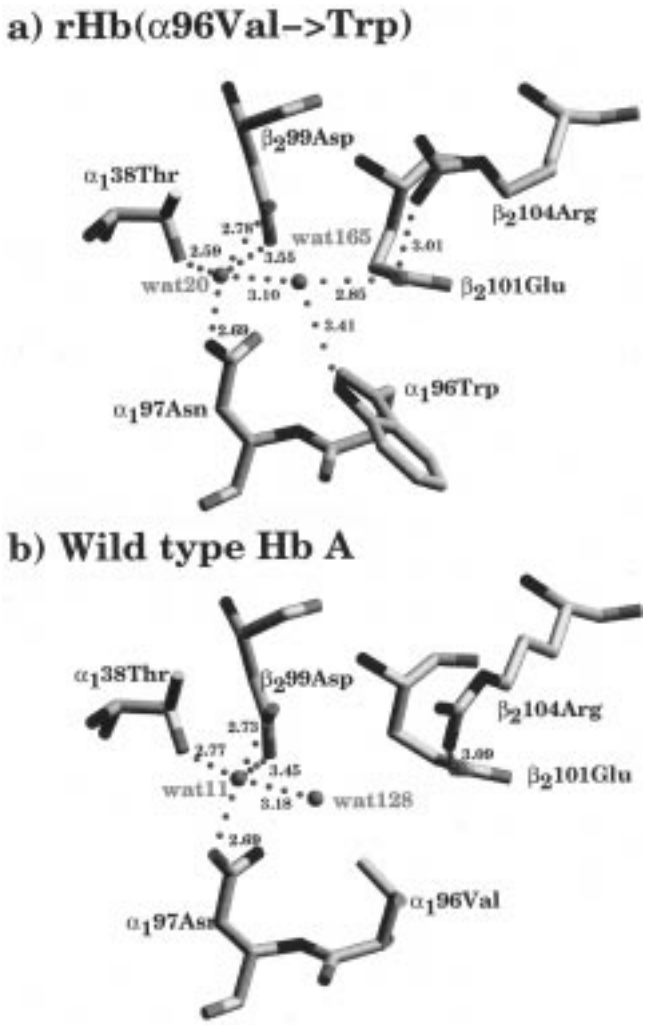

FIGURE 3: The local hydrogen-bonding network in the T-state structure in (a) rHb (α96Val→Trp) and (b) wild-type Hb A [2HHB (*18*)]. Possible hydrogen bonds or electrostatic interactions shorter than 3.6 Å are shown. Distances are in angstroms. Figure produced with SETOR (*38*).

Heme Ligands. In the T-state structure, strong spherical electron density was seen between the heme iron and the distal histidine αHis58 in each α chain, but no such density was observed in the β chains, suggesting an α-aquomet, β-deoxy T-state (Figure 1, panels a and b). This is in accord with the prior observation from another α-met, β-deoxy T-state Hb A structure that there is "a clear preference for binding ligand to the α heme groups in the high-salt T-state crystal" (*20*). In the R-state, strong ellipsoidal density between the iron of both the α and β hemes and the distal histidines α58His and β63His was modeled as carbon monoxide (Figure 1c).

α*96Trp in the T-State Interface.* Both the initial difference Fourier and subsequent simulated annealing OMIT maps show strong density for the α96Trp side chains in the T-state structure (Figure 2a). However, the side chain adopts an orientation different from that predicted by Kim et al. (*6*) (Figure 2a, Table 2), and there is no evidence for the hydrogen bonds between α96Trp and β99Asp that were predicted to stabilize the T-state. Instead, water-mediated hydrogen bonds between α96Trp Nε1 and β101Glu Oε2 are observed to span both the $\alpha_1-\beta_2$ and $\alpha_2-\beta_1$ interfaces (Figure 3a). Since the asymmetric unit contains the full $\alpha_2\beta_2$ tetramer, these two observations of a water-mediated hydrogen bond are essentially independent and are thus unlikely to be an artifact of crystallization.

Table 2: Side-Chain Dihedral Angles of α96Trp in rHb (α96Val→Trp)[a]

	T-state	closest rotamer	|difference in χ|
	crystal structure		
$\alpha_1$96Trp			
χ_1	171.6	−177.3	11.1
χ_2	−114.9	−95.1	19.8
$\alpha_2$96Trp			
χ_1	162.3	−177.3	20.4
χ_2	−114.2	−95.1	19.1
	T-state	predicted rotamer	|difference in χ|
	simulation		
$\alpha_1$96Trp			
χ_1	92.3	64.8	27.5
χ_2	−71.0	−88.9	17.9
$\alpha_2$96Trp			
χ_1	96.2	64.8	31.4
χ_2	−78.7	−88.9	10.2

[a] The "closest rotamer" is the rotamer from the Ponder and Richards (*28*) library closest to the values obtained from the crystal structure, and has a tabulated incidence of 13.8%; the "predicted rotamer" was that thought to be closest to the natural conformation by Kim et al. (*6*) and has a tabulated incidence of 20.7%. The simulated T-state angles were those calculated by Kim et al. by a 10 ps MD simulation with the predicted rotamer as the starting conformation.

Each α96Trp appears to be solvated in the central cavity (Figure 6a), with essentially identical χ_1 and χ_2 angles for 96Trp in both the α_1 and α_2 subunits (Table 2). Both side chains are well-ordered, with average side-chain *B*-factors of 31.1 Å^2 for $\alpha_1$96Trp and 31.6 Å^2 for $\alpha_2$96Trp. One water molecule is hydrogen-bonded to each indole nitrogen (Figures 2a, 3a, and 6a): water 165 (B = 39.9 Å^2) is 3.4 Å from the $\alpha_1$96Trp Nε1, and water 190 (B = 43.0 Å^2) is 2.9 Å from the $\alpha_2$96Trp Nε1. The only other additional interactions of α96Trp are van der Waals contacts with the aliphatic portion of the side chains of αLys99 and αLeu100, as well as with βGlu101 (discussed below).

It appears that hydrogen bonds with ordered solvent molecules constitute the most significant interactions of α96Trp, which may be involved in stabilizing the T-state dimer−dimer interface. The water bound to α96Trp Nε1 is within hydrogen-bonding distance of the carboxylate of β101Glu, the hydroxyl of αThr38, and a second water. This second water (water 20 at the $\alpha_1-\beta_2$ interface, water 28 at the $\alpha_2-\beta_1$ interface) interacts with the side-chain carboxylate oxygens of β99Glu and the Nδ2 of αAsn97 (Figure 3a). Both water molecules have been seen at similar locations in the 1.74 Å deoxy T-state (2HHB) structure (Figure 3b).

This hydrogen-bonding network is similar to that observed in the wild-type T-state structure. A major difference is seen in both β101Glu side chains, where rotations resulting in dihedral angles of approximately $\chi_1 = -85°$, $\chi_2 = -50°$ (Figures 3 and 4a) permit the water-mediated hydrogen bond with α96Trp. This motion also allows for the formation of novel van der Waals interactions between the βGlu101 side chain and the Cβ, Cγ, Cδ1, and Nε1 atoms of the indole ring. Among 11 other T-state structures surveyed, the conformation of β101Glu was consistently found to cluster around $\chi_1 = 180°$ and $\chi_2 = 60°$ (Figure 4a), so this motion is likely to be a consequence of the mutation.

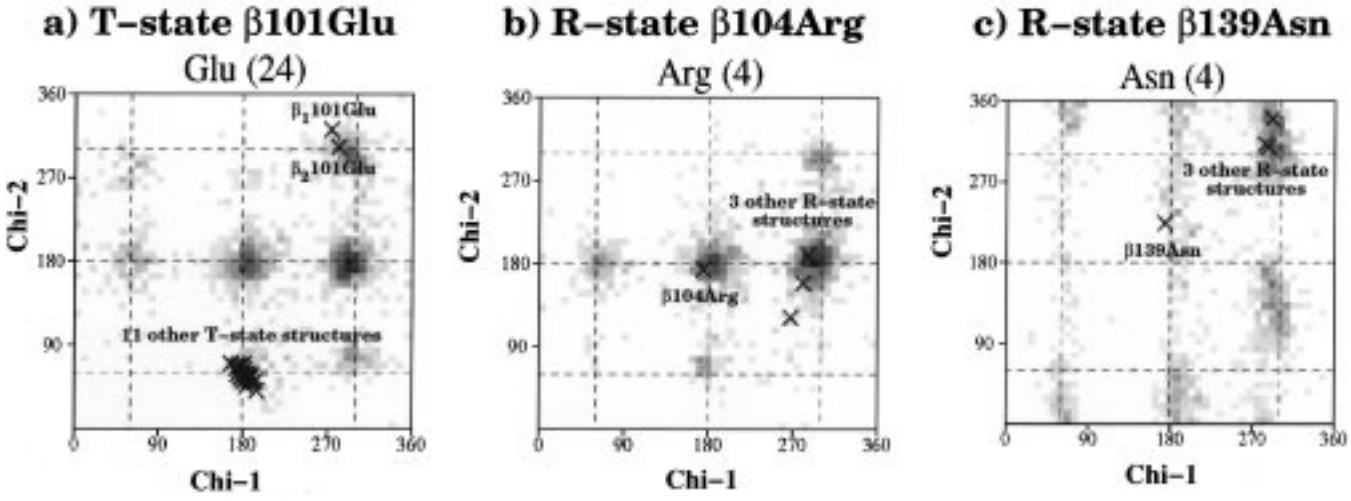

FIGURE 4: (a) Side-chain dihedral angles of $\beta_1$101Glu and $\beta_2$101Glu in T-state rHb (α96Val→Trp) compared with the dihedral angles of those same residues in 11 other T-state structures (1CLS, 1DSH, 1DXU, 1DXV, 1HBB, 1HGA, 1HGB, 1HGC, 1SDK, 1THB, 2HHB). The two data points around (315°, 315°) are from rHb (α96Val→Trp). (b) Side-chain dihedral angles of β104Arg in the R-state structure of rHb (α96Val→Trp) compared with the dihedral angles of the same residue in three other R-state structures (1HHO, 2HCO, 2HBC). The data point at (180°, 180°) is from rHb (α96Val→Trp). (c) Plot of the side-chain dihedral angles of β139Asn in R-state rHb (α96Val→Trp) compared to other R-state structures. The data point at (180°, 225°) is from rHb (α96Val→Trp). Diagrams generated with PROCHECK (*16*).

In wild-type Hb A, β101Glu participates in an electrostatic interaction with β104Arg, which has been implicated in stabilizing the T-state structure (*24*). Although there is a large movement of β101Glu in both dimers, each β104Arg has moved in a compensatory fashion so that the electrostatic interaction is preserved (Figure 3).

α96Trp in the R-State Structure. Figure 2b shows the conformation of α96Trp in the R-state structure of rHb (α96Val→Trp). Although it is not as well-ordered as in the T-state structure, with an average temperature factor of 51.4 Å^2, the initial difference Fourier map and OMIT map density clearly show its orientation (Figure 2b), where it is also solvated in the central cavity (Figure 6b).

In the R-state, the tryptophan has a few interactions with other residues. Its closest neighbor is β101Glu, with which it makes two contacts of 3.4 and 3.9 Å; these may be equatorial oxygen−aromatic interactions, where the $\delta-$ of the Oϵ1 and Oϵ2 atoms favorably interacts with the $\delta+$ of the equatorial hydrogens on the conjugated ring (*25*). The remaining interactions appear to be van der Waals contacts with α99Lys (3.5 Å), β99Asp (3.6 Å), β101Glu (3.7 Å), β104Arg (3.6 Å) (Figure 5a), and a 3.8 Å closest approach to its symmetry mate across the solvent cavity (Figure 6b).

The side chains of β104Arg and β139Asn adopt conformations different from those modeled in other R-state structures (Figure 4, panels b and c). It is possible that the van der Waals or weakly polar interactions with α96Trp stabilize the observed conformation of β104Arg, disrupting its previous hydrogen bonds with β139Asn, but gaining two electrostatic interactions with β101Glu (Figure 5). Thus freed, β139Asn is allowed to pivot and make 3.4−3.6 Å contacts with both $\beta_1$146His and $\beta_2$146His.

DISCUSSION

Structural Basis for Lower Oxygen Affinity. In the original analysis by Kim et al. (*6*), a preliminary molecular dynamics simulation suggested that, in the T-state of rHb (α96Val→Trp), α96Trp would adopt an orientation where its indole Nϵ would interact with both carboxylate oxygens of β99Asp. It was predicted that these new hydrogen bonds at the $\alpha_1-\beta_2$ interface would stabilize the T-state, thus resulting in a lower oxygen affinity for the mutant protein. Measurements of the P_{50} showed that the oxygen affinity was decreased and the new equilibrium between T- and R-states was consistent with the existence of these four (two per $\alpha\beta$ dimer) hydrogen bonds. However, in the crystal structures, α96Trp does not make direct hydrogen bonds across the dimer−dimer interface. Instead, the side-chain torsion angles are such that the whole ring is directed away from the interface and into the central cavity, and α96Trp is found to make a water-mediated hydrogen bond with β101Glu (Figures 3a and 6a). Although the water molecule involved in this hydrogen bond has been seen in approximately the same location in deoxy Hb A (*18*), β101Glu is in a conformation significantly different from that observed previously in other T-state structures (Figures 3 and 4a). The most likely explanation for the reorientation of β101Glu is that the introduction of α96Trp induced the 0.45−0.55 Å movement of water 165/190, bringing it to a location which favors β101Glu to adopt this new conformation. It is also possible that novel van der Waals interactions with the indole ring of α96Trp also contributed to the stability of the conformation of βGlu101.

Although the predicted hydrogen bonds have not been observed, a different set of four inadvertently engineered hydrogen bonds has been observed: $\alpha_1$96Trp−Wat165, Wat165−$\beta_2$101Glu, $\alpha_2$96Trp−Wat190, and Wat190−β_1-101Glu (Figures 3 and 6a). Since these interactions do not exist in the wild-type T-state, they may serve to stabilize the T-state of the mutant protein. This is a plausible explanation for the shift of equilibrium toward the T-state for rHb (α96Val→Trp), particularly since water structure has been shown to be crucial in stabilizing the low-affinity conformation of the dimeric hemoglobin HbI from *Scapharca inaequivalvis*, where 6 of 17 ordered water molecules at the deoxy interface are displaced upon oxygenation (*26*). Although the α72Thr→Val mutation of HbI does change the

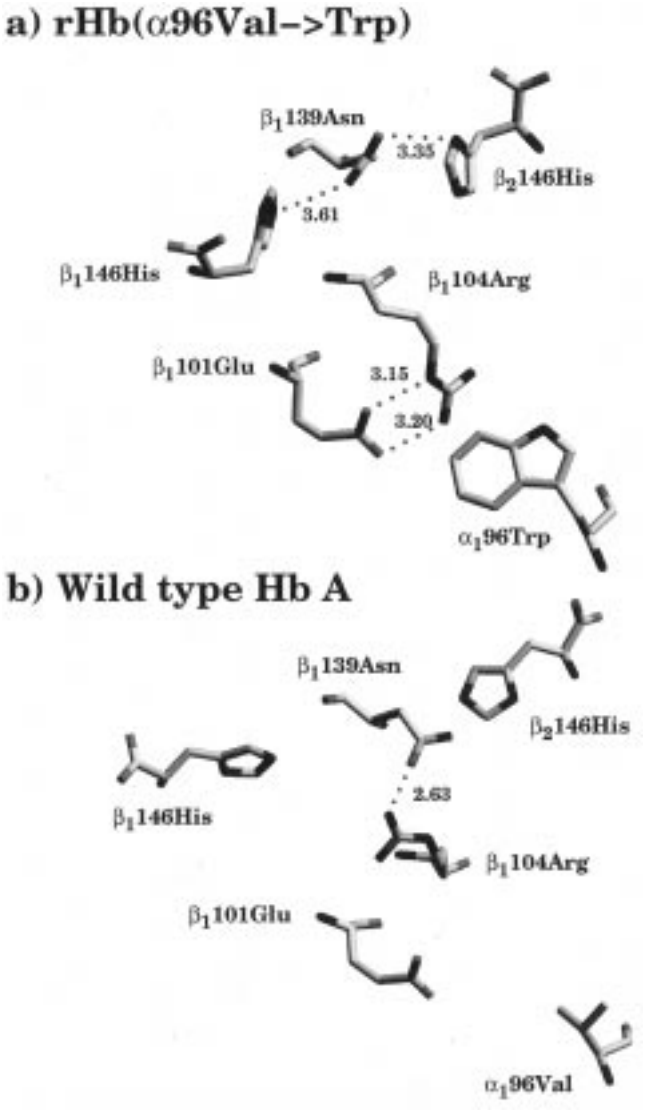

FIGURE 5: Residues β101Glu and β104Arg and their neighbors in the R-state crystal structures of (a) rHb (α96Val→Trp) and (b) wild-type oxy Hb A [1HHO (*10*)]. Possible hydrogen bonds or electrostatic interactions shorter than 3.6 Å are shown. Distances are in angstroms. Figure produced with SETOR (*38*).

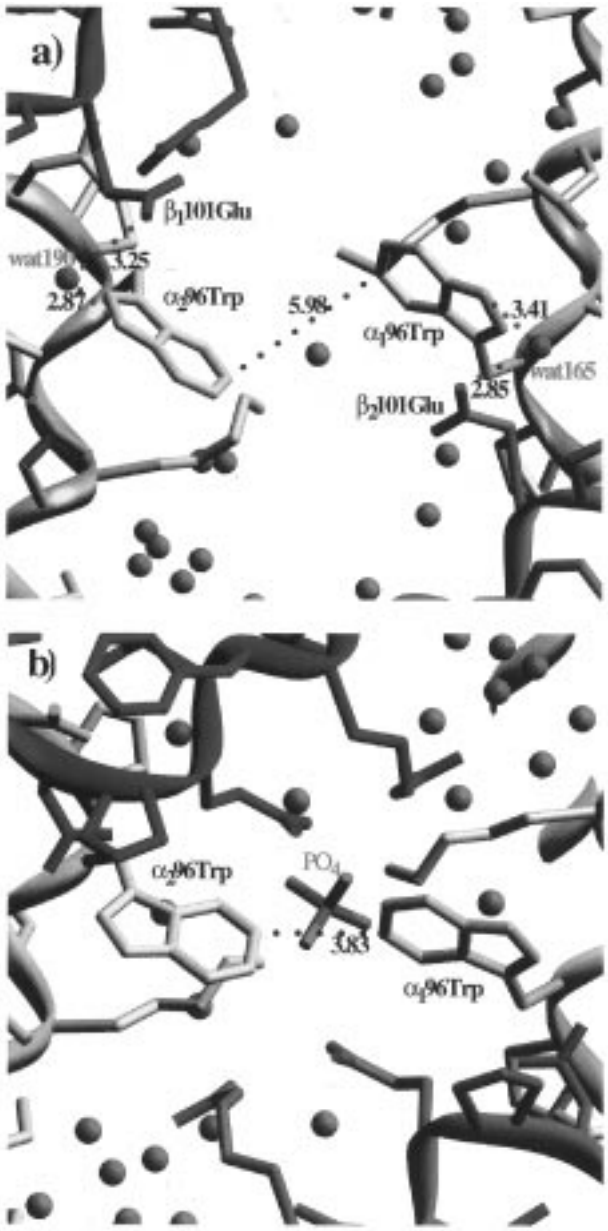

FIGURE 6: The two α96Trp residues in the solvent cavity in the (a) T-state structure and (b) R-state structure. The view is approximately down the 2-fold axis relating the $\alpha\beta$ dimers. The subunits are colored white for α_1, green for β_1, yellow for α_2, and purple for β_2. Distances are in angstroms. Figure produced with SETOR (*38*).

equilibrium between the liganded and free forms, it does so by *abolishing* water-mediated hydrogen bonds and *destabilizing* one conformation, the deoxy state (*26*), thus increasing ligand affinity. Conversely, the T-state of (α96Val→Trp) appears to be the first such instance where a site-directed mutation *creates* new water-mediated hydrogen bonds to *stabilize* one conformation of an allosteric protein, in this case the deoxy state, thus decreasing ligand affinity. Ideally, the osmotic shock experiments of Royer et al. (*26*) would confirm that the two waters bridging the T-state interface also function as allosteric effectors, but it is unlikely that the method is sensitive enough to detect a difference of two water molecules among the 60 or so which Hb gains upon making the transition from the T-state to the R-state (*27*).

An additional difference between the wild-type and mutant structures can be seen in the existence of a novel electrostatic interaction between β101Glu and β104Arg in the R-state, an interaction which was previously proposed to be important in stabilizing the T-state on the basis of four β101 mutants with increased oxygen affinity (*24*). Although this salt bridge is observed in the wild-type T-state and is preserved in the mutant T-state even though β101Glu has moved significantly (Figure 3), this interaction has not been observed in other R-state structures until now. Unlike the corresponding residue in three other R-state structures (Figure 4b), in rHb-(α96Val→Trp), β104Arg has moved to form two 3.2 Å salt bridges with β101Glu, presumably due to van der Waals and weakly polar contacts with α96Trp (Figure 5). Although the mechanism by which this electrostatic interaction influences hemoglobin structure and dynamics has not been established, if the molecule must gain the β101Glu−β104Arg bond as it progresses along the reaction coordinate from R-state to T-state, the presence of this interaction in the R-state of rHb(α96Val→Trp) might impart a slightly "T-like" character, i.e., the molecule would be farther along the reaction coordinate toward the T-state. Since the precise

nature of the importance of β101Glu in stabilizing the T-state is not understood [although, see Abraham et al. (*20*) for a proposed explanation], the importance of these salt bridges in the altered oxygen affinity of the mutant Hb cannot be evaluated.

Hydration in Molecular Dynamics Studies. In the original molecular dynamics simulations, the starting points were the most common tryptophan rotamers from the library of Ponder and Richards (*28*), so it came as a surprise that not only was an incorrect conformation predicted but the crystallographically observed conformation is close to a rotamer which is observed with an incidence of 13.8% (Table 2). The computational prediction may be due to the omission of crystallographically bound waters in the simulation. The waters observed to mediate a hydrogen bond between α96Trp and β101Glu are observed in the wild-type T-state structure (Figure 3), so it is possible that the inclusion of these ordered solvent molecules might have stabilized the $\chi_1 = -177.3$ and $\chi_2 = -95.1$ rotamer experimentally observed in the T-state structure.

It should not come as surprise that some ordered water molecules are bound tightly enough to this protein that they must be considered an integral part of the protein structure (*29*). In a number of crystallographic studies (*30*, *31*; also see the studies reviewed by Ringe in ref *32*), water molecules have been observed to remain tightly bound to the surface of proteins such as elastase even when bulk water is displaced by an organic solvent. Furthermore, computational and crystallographic studies of ribonuclease A (*33*) show that the proper characterization of binding sites on the surface of a protein may be dependent upon the inclusion of solvent molecules as part of that surface.

It is clear that a continuum model of solvent will not suffice for molecular dynamics studies of proteins such as rHb(α96Val→Trp) in which ordered solvent molecules play a crucial role in the structure and function of the protein. However, approaches which randomly fill space with discrete solvent molecules, such as the original MD study of rHb-(α96Val→Trp), may also fail with these very same proteins if they do not include the relevant ordered solvent molecules at the correct locations. Proper modeling of ordered solvent will be necessary for calculations involving other allosteric proteins, as in the example of phosphopfructokinase, which requires the formation of a layer of ordered water molecules upon making the T to R transition (*34*).

Ideally, before performing MD calculations for a protein, there should be a list of crystallographically observed solvent molecules which are considered to be part of the protein structure for the purposes of the simulation. The trouble lies in deciding which of these molecules are "crucial" for the simulation, although an indication may be provided if a particular water molecule remains ordered and bound to the protein in a crystal where the aqueous mother liquor has been exchanged for an organic solvent (*32*) or whether a given solvent molecule is present in multiple crystal forms of the protein (*35*). Since these approaches are impractical for most protein crystals, an alternative measure might be to include all crystallographically observed water molecules with a temperature-factor below a certain threshold, although the choice of this cutoff would be arbitrary. Future MD studies should compare results of simulations with continuum solvent models, with random solvent models, and with crystallographically observed solvent molecules that are chosen by various criteria.

Future Design of Blood Substitute Candidates. The findings reported here have provided further confirmation of our hypothesis that selective stabilization of the T-state should yield mutant Hbs with lowered oxygen affinity and unimpaired cooperativity (*5*). The double mutant (α96Val→Trp, β108Asn→Lys) has been recently constructed and found to have an even lower oxygen affinity than either rHb-(α96Val→Trp) or rHb Presbyterian (β108Asn→Lys) (*5*). Further design of low-affinity Hb derivatives will proceed along similar lines, combining MD, NMR, and crystallography, for the purpose of amassing a library of mutations which stabilize the T-state and do not disturb the R-state, and then rationally combining these mutants to attain even more desirable oxygen-carrying proteins.

ACKNOWLEDGMENT

The authors would like to thank Dr. J. Friedman, Dr. D. Gottfried, and Dr. E. Peterson for stimulating discussions.

REFERENCES

1. Bunn, H. F. (1993) *Am. J. Hematol. 42*, 112−117.
2. Winslow, R. M. *Hemoglobin-Based Red Cell Substitutes*, Johns Hopkins University Press, Baltimore, 1992.
3. Winslow, R. M. (1997) *Sci. Med. 4*, 54−63.
4. Shen, T.-J., Ho, N. T., Simplaceanu, V., Zou, M., Green, B. N., Tam, M. F., and Ho, C. (1993) *Proc. Nat. Acad. Sci. U.S.A. 91*, 11547−11551.
5. Ho, C., Sun, D. P., Shen, T.-J., Ho, N. T., Zou, M. Hu, C. K., Sun, Z.-Y., and Lukin, J. L. (1997) Recombinant Hemoglobins with Low Oxygen Affinity and High Cooperativity. In *Present and Future Perspectives or Blood Substitutes* (Tsuchida, E., Ed.) Elsevier Science SA, Lausanne, Switzerland.
6. Kim, H. W., Shen, T. J., Sun, D. P., Ho, N. T., and Ho, C. (1995) *J. Mol Biol. 248*, 867−882.
7. Perutz, M. F. (1969) *J. Crystal Growth 2*, 54−56.
8. Kabsch, W. (1988) *J. Appl. Crystallogr. 21*, 916−924.
9. Kavanaugh, J. S., Rogers, P. H., and Arnone, A. (1992) *Biochemistry 31*, 8640−8647.
10. Shaanan, B. (1983) *J. Mol. Biol. 171*, 31−59.
11. Brünger, A. T. (1993) *X-PLOR (version 3.1) Manual*, Yale University, New Haven, CT.
12. Jones, T. A. (1985) *Methods Enzymol. 15*, 157−171.
13. Jones, T. A., Zhou, J.-Y., Cowan, S. W., and Kjeldgaard, M. (1991) *Acta Crystallogr., Sect. A 47*, 110−119.
14. Hodel, A., Kim, S.-H., and Brünger, A. T. (1992) *Acta Crystallogr., Sect. A 48*, 851−858.
15. Jiang, J. S., and Brünger, A. T. (1994) *J. Mol. Biol. 243*, 100−115.
16. Laskowski, R. A., MacArthur, M. W., Moss, D. S., and Thornton, J. M. (1993) *J. Appl. Crystallogr. 26*, 283−291.
17. Vriend, G. (1990) *J. Mol. Graph. 8*, 52−56.
18. Fermi, G., Perutz, M. F., Shaanan, B., and Foure, R. (1984) *J. Mol. Biol. 175*, 159−174.
19. Brzozowski, A., Derewenda Z., Dodson, E., Dodson, G., Grabowski, M., Liddington, R., Skarzynski, T., Vallely D. (1984) *Nature 307*, 74−76.
20. Abraham, D. J., Peascoe, R. A., Randad, R. S., and Panikker, J. (1992) *J. Mol. Biol. 227*, 480−492.
21. Liddington, R., Derewenda, Z., Dodson, E., Hubbard, R., and Dodson, G. (1992) *J. Mol. Biol. 228*, 551−579.
22. Liddington, R. (1994) *Methods Enzymol. 232*, 15−26.
23. Baldwin, J. M. (1980) *J. Mol. Biol. 136*, 103−128.
24. Shih, D. T.-b., Jones, R. T., Imai, K., and Tyuma, I. (1985) *J. Biol. Chem. 260*, 5191−5924.
25. Burley, S. K., and Petsko, G. A. (1988) *Adv. Protein Chem. 39*, 125−189.

26. Royer, W. E. Jr., Pardanani, A., Gibson, Q. H., Peterson, E. S., and Friedman, J. M. (1996) *Proc. Natl. Acad. Sci. U.S.A. 93*, 14526−14531.
27. Colombo, R. F., Rau, D. C., and Parsegian, V. A. (1992) *Science 256*, 655−659.
28. Ponder, J. W., and Richards, F. M. (1987) *J. Mol. Biol. 193*, 775−791.
29. Baker, E. N. (1995) Solvent Interactions with Proteins as Revealed by X-Ray Crystallographic Studies. In *Protein−Solvent Interactions* (Gregory, R. B.; Ed.) Chapter 2, Marcel-Dekker, New York.
30. Yennawar, N. H., Yennawar, H. P., and Farber, G. K. (1994) *Biochemistry 33*, 7326−7336.
31. Schmitke, J. L., Stern, L. J., and Klibanov, A. M. (1997) *Proc. Nat. Acad. Sci. U.S.A. 94*, 4250−4255.
32. Ringe, D. (1995) *Curr. Opin. Struct. Biol. 5*, 825−829.
33. Joseph-McCarthy, D., Fedorov, A. A., and Almo, S. C. (1996) *Protein Eng. 9*, 773−780.
34. Schirmer, T., and Evans, P. R. (1990) *Nature 343*, 140−145.
35. Zhang, X. J., and Matthews, B. W. (1994) *Protein Sci. 3*, 1031−1039.
36. Engh, R. A., and Huber, R. (1991) *Acta Crystallogr., Sect. A 47*, 392−400.
37. Martin, A. C. R. (1995) *ProFit V1.6: Protein Least Squares Fitting*, SciTech Software, Ashtead, Surrey, U.K.
38. Evans, S. V. (1993) *J. Mol. Graph. 11*, 134−138.

BI9727287